

Bayesian Optimisation using microscopic and integral measurements to infer nuclear data parameters

Daan Houben, Mathieu Hursin

December 10, 2025

Abstract

test 123

1 Introduction

Nuclear data is considered as the major source of uncertainty in some reactor observables, most notably effective multiplication factor (k_{eff}). The nuclear data available in evaluated nuclear data libraries, such as cross sections, neutron multiplicities, angular distributions or fission neutron energy spectrum, are a result of a complex fitting procedure including theoretical models, microscopic experiments and expert judgement. Integral experiments are then used to assess the performance of the nuclear data. In this work, a Bayesian Optimization (BO) framework is proposed which enables consolidating microscopic energy dependent measurements with integral experiments to estimate nuclear data parameters.

The BO is performed using a Markov Chain Monte Carlo (MCMC) method in which surrogates are used to evaluate the likelihoods. For the microscopic energy dependent measurements, the SAMMY v8.1.0 resonance fitting tool [1] is employed. While SERPENT v2.2.2 [2], a Monte Carlo neutron transport code, is used to quantify the integral response. Surrogates are trained by evaluating random samples drawn in the input space in the high-fidelity models. The methodology is tested on two case studies, being ^{53}Cr and ^{238}U . Since microscopic experiments often provide many points and integral experiments only provide a single points, care is given to analyze how different assumptions regarding the likelihood evaluation affect the posterior.

2 Background and mathematical motivation

2.1 Bayesian Optimisation setup

The main objective of this paper is to infer nuclear data parameter(s) from a set of both microscopic energy dependent an integral experiments. Microscopic energy dependent measurements, further noted as microscopic measurements, are measurements of single energy neutron properties. Often such measurements result from neutron Time-Of-Flight (nTOF) facilities in which the energy of the neutron is derived from the time it takes for the neutron to reach a target. Typical of these measurements is the many measurement points that are obtained. In contrast, integral measurements such as criticality experiments, only provide one value which is representative of a group of nuclides, reactions and energies.

According to Bayes theorem, the posterior (updated) probability density function (PDF), $P(\theta|\text{data})$, is proportional to the likelihood of observing the parameter(s) θ given the data multiplied by the prior belief of the parameter(s):

$$P(\theta|\text{data}) \propto P(\text{data}|\theta) \cdot P(\theta) \quad (1)$$

For brevity, we shall refer to the likelihood as $\mathcal{L}(\theta) = P(\text{data}|\theta)$.

2.2 Markov Chain Monte Carlo (MCMC)

To calculate the posterior distribution, various techniques can be derived from Bayes theorem. Popular techniques include Generalized Linear Least Squares (GLLS), Bayesian Monte Carlo (BMC), MOCABA, etc. In this paper, an algorithm belonging to the family of Markov Chain Monte Carlo (MCMC) techniques is selected. As MCMC is a name for a family of techniques, first the general principle is explained, after which the Emcee algorithm used in this paper is detailed.

In most MCMC algorithms, the unnormalized posterior is evaluated to generate samples:

$$P^*(\theta|\text{data}) = \mathcal{L}(\theta) \cdot P(\theta) \quad (2)$$

where $P^*(\theta|\text{data})$ represents the posterior up to a normalizing constant. The objective is to construct a Markov chain $\{\theta_0, \theta_1, \dots, \theta_N\}$ such that the stationary distribution of the chain converges to the posterior distribution $P(\theta|\text{data})$. Under the assumption of Normally distributed prior ($\mathcal{N}(\theta_0, \Sigma)$) and likelihood ($\mathcal{N}(\mathbf{y}_{\text{true}}, \mathbf{A})$), the unnormalized posterior probability evaluated at θ can be rewritten as

$$P^*(\theta|\text{data}) = \frac{1}{\sqrt{(2\pi)^m \det \mathbf{A}}} \exp \left[-\frac{1}{2} (\mathbf{f}(\theta) - \mathbf{y}_{\text{exp}})^T \mathbf{A}^{-1} (\mathbf{f}(\theta) - \mathbf{y}_{\text{exp}}) \right] \times \frac{1}{\sqrt{(2\pi)^n \det \Sigma}} \exp \left[-\frac{1}{2} (\theta_0 - \theta)^T \Sigma^{-1} (\theta_0 - \theta) \right] \quad (3)$$

in which the first term represents the probability of observing θ given the measurements, with \mathbf{y}_{exp} is the vector describing the m measurement points, $\mathbf{f}(\theta)$ is the vector containing the model responses for the vector θ and \mathbf{A} is the covariance matrix describing the measurement points of size $(m \times m)$. The prior probability evaluated at θ can then be calculated using the prior belief of the n parameters θ_0 , with covariance matrix Σ of size $(n \times n)$.

Standard algorithms, such as Metropolis-Hastings, propose a new state θ' based on a proposal distribution $q(\theta'|\theta_t)$ and accept it with probability $\alpha = \min(1, \frac{P^*(\theta')q(\theta_t|\theta')}{P^*(\theta_t)q(\theta'|\theta_t)})$. However, in high-dimensional nuclear data spaces where parameters may be highly correlated, standard proposal distributions often result in poor mixing.

For ease of tuning and implementation as well as future proofing, we employ the Affine Invariant Ensemble Sampler (AIES), as implemented in the *emcee* code [3]. In this algorithm, an ensemble of K "walkers" are propagated in parallel. The proposal step for a walker θ_k is based on the current position of a complementary walker θ_j from the ensemble:

$$\theta'_k = \theta_j + Z(\theta_k - \theta_j) \quad (4)$$

where Z is a scaling variable drawn from a distribution $g(z) \propto 1/\sqrt{z}$ on the interval $[1/a, a]$. This "stretch move" allows the algorithm to efficiently sample distributions with strong correlations without requiring manual tuning of the covariance matrix of the proposal distribution, making it straightforward to implement.

2.3 Likelihood Formulation

The formulation of the likelihood function $\mathcal{L}(\theta)$ is one of the main challenges when combining integral and microscopic data, as the magnitude of data points differs by orders of magnitude, hereby possibly diluting the effect of the integral measurement. To try and understand better to which extend the diluting effect of the microscopic measurements affects the useability of

the integral measurements, different possibilities to approach the covariance matrix of the measurement points are analyzed. First and foremost, the correct and most rigour method is to use the real covariance matrix describing the measurement points. However, this is often seen as too complex. Especially, calculating experimental correlations between integral experiments and inbetween microscopic and integral experiments. In this regard, the first assumption comes into play, i.e., there are no correlations between microscopic and integral experiments and no correlations between integral experiments. This assumption may not be valid when integral experiments from the same facility are used, therefore, we limit our analysis by only regarding integral experiments from different facilities. This assumption should be sufficiently valid regarding the correlations due to nuclear data will dominate. Now, it is possible to calculate the total likelihood $\mathcal{L}(\theta)$ for θ for the set of microscopic experiments J and integral experiments I using

$$\begin{aligned} \mathcal{L}(\theta) = \prod_{j \in J} \frac{1}{\sqrt{(2\pi)^{m_j} \det \mathbf{A}_j}} \exp \left[-\frac{1}{2} (\mathbf{f}_j(\theta) - \mathbf{y}_j)^T \mathbf{A}_j^{-1} (\mathbf{f}_j(\theta) - \mathbf{y}_j) \right] \times \\ \prod_{i \in I} \frac{1}{\sqrt{2\pi\sigma_i^2}} \exp \left[-\frac{(f_i(\theta) - y_i)^2}{2\sigma_i^2} \right] \end{aligned} \quad (5)$$

As probabilities are often very small numbers, the natural logarithm is taken to preserve numerical stability. The log-likelihood $\ln \mathcal{L}(\theta)$ then becomes

$$\begin{aligned} \ln \mathcal{L}(\theta) = -\frac{1}{2} \sum_{j \in J} \ln [(2\pi)^{m_j} \det \mathbf{A}_j] + -\frac{1}{2} \sum_{j \in J} [(\mathbf{f}_j(\theta) - \mathbf{y}_j)^T \mathbf{A}_j^{-1} (\mathbf{f}_j(\theta) - \mathbf{y}_j)] + \\ -\frac{1}{2} \sum_{i \in I} \ln [2\pi\sigma_i^2] + -\frac{1}{2} \sum_{i \in I} \frac{(f_i(\theta) - y_i)^2}{\sigma_i^2} \end{aligned} \quad (6)$$

Now two approximations are analyzed, i.e. (1) all microscopic measurement points behave independently and (2) the correlation between all microscopic measurements points of a single experiment is 1 and there is no experimental correlation between the experiments.

2.3.1 Independent microscopic measurement points

When all measurement points behave independently, each datapoint has the same weight as an integral experiment. In this sense, integral experiments will be diluted and their influence on the posterior is expected to be negligible. Nevertheless, the loglikelihood for independent microscopic experiments from Eq. 6 therefore becomes

$$\begin{aligned} \ln \mathcal{L}_J(\theta) = -\frac{1}{2} \sum_{j \in J} \sum_{e \in E_j} \ln [2\pi\sigma_{j,e}^2] + -\frac{1}{2} \sum_{j \in J} \sum_{e \in E_j} \left[\frac{(f_{j,e}(\theta) - y_{j,e})^2}{\sigma_{j,e}^2} \right] \\ = C - \frac{1}{2} \sum_{j \in J} \chi_j^2 \end{aligned} \quad (7)$$

in which $\chi^2 = \sum \frac{(y_c - y_e)^2}{\sigma_e^2}$ is the chi-squared goodness-of-fit for the datapoints resulting from an experiment. Since the term $-\frac{1}{2} \sum_{j \in J} \sum_{e \in E_j} \ln [2\pi\sigma_{j,e}^2]$ does not depend on θ , it can be calculated beforehand and replaced by a constant C .

2.3.2 Fully correlated microscopic measurement points

Now the opposite is assumed and all microscopic measurement points are expected to be highly correlated. Then, we take the chi-squared per degree of freedom, so Eq. 6 becomes

$$\begin{aligned}\ln \mathcal{L}_J(\theta) &= -\frac{1}{2} \sum_{j \in J} \frac{1}{N} \sum_{e \in E_j} \ln [2\pi\sigma_{j,e}^2] + -\frac{1}{2} \sum_{j \in J} \frac{1}{N} \sum_{e \in E_j} \left[\frac{(f_{j,e}(\theta) - y_{j,e})^2}{\sigma_{j,e}^2} \right] \\ &= -\frac{1}{2} \sum_{j \in J} 2\pi\bar{\sigma}_j^2 - \frac{1}{2} \sum_{j \in J} \chi_j^2/N \\ &= C - \frac{1}{2} \sum_{j \in J} \chi_{N,j}^2\end{aligned}\tag{8}$$

here, $\bar{\sigma}_j$ is the average experimental uncertainty and $\chi_{N,j}^2$ is the chi-squared per degree of freedom for microscopic experiment j .

2.4 Surrogate Modelling

The MCMC algorithm requires several thousands of likelihood evaluations to explore the posterior distribution effectively and reach convergence. Directly executing high-fidelity codes, i.e., SAMMY for resonance fitting and SERPENT for Monte Carlo neutron transport, at each step of the chain is computationally expensive. To overcome this bottleneck, we employ surrogate models that mimic the response of the high-fidelity physics codes within the training space.

In this work, Gaussian Process (GP) regression is selected as the surrogate modelling technique. Conceptually, a Gaussian Process can be understood as a non-parametric method that does not fit a single specific function to the data, but rather defines a probability distribution over all possible functions that are consistent with the observed data.

One of the main benefits of a GP is that it provides both a predicted mean value and an associated uncertainty (variance) for every point in the input space. This feature is particularly valuable in Bayesian optimization, as it quantifies the surrogate's confidence, ensuring that the MCMC sampler does not become overconfident in regions where training data is sparse. The behavior of the GP is primarily governed by a covariance function, or *kernel*, which mathematically defines the similarity between data points: points closer in the input space are assumed to have more strongly correlated outputs.

To train the surrogates, a dataset is generated by drawing uniform random samples across a wide input space. These samples are propagated through the high-fidelity models to obtain the true responses. For microscopic experiments, SAMMY is used to calculate the goodness-of-fit metric (χ^2). For integral experiments, SERPENT is used to calculate the effective multiplication factor k_{eff} . The resulting dataset of in-/output is randomly divided, with 80% used for training the GPs and the remaining 20% is used for testing purposes.

The choice of the kernel function is important to train the GP and predict new points. We use a Radial Basis Function (RBF) kernel to train the GP for integral experiments since our data k_{eff} behaves smoothly with variations in input space. The RBF kernel is suitable for linear and smooth non-linear functions. For microscopic measurements, the SAMMY code is used to calculate a goodness-of-fit metric, i.e., χ^2 , which behaves as a quadratic function with a minimum. Therefore, we use a polynomial kernel of second degree. A white noise kernel is added in both cases, for integral experiments it is added to account for the statistical uncertainty of the Monte Carlo method. While the microscopic experiments use a deterministic method to calculate the goodness-of-fit, a small white noise kernel is added to ensure positive definitiveness of the covariance matrix to account for numerical instabilities.

The reliability of the surrogates is assessed before use in the MCMC sampler. The validation involves inspecting parity plots (predicted vs. true values in the testing set), analyzing the distribution of residuals, and examining 1D slice plots.

2.5 Including uncertainties of other nuclides

When performing a Bayesian Optimization, uncertainties of other nuclides should also be taken into account in order not to correct for bias induced by other sources. For criticality experiments, these other nuclear data uncertainties are estimated using relative first-order sensitivity coefficients calculated using Serpent-2. Here, sensitivity coefficients describing the effect of nuclear data perturbations on k_{eff} in ECCO-33 multi-group energy structure are calculated using Generalized Perturbation Theory (GPT) [4] for all nuclides in the system of consideration and for the reactions fission, capture, in/elastic scattering, neutron fission multiplicities and prompt neutron fission energy spectrum. The relative sensitivity vectors are included in a matrix, $S_{k,\sigma}$, for the integral experiments under consideration. Then using SANDY [5], wrapping the NJOY2016 code [6], covariance matrices Σ_σ were generated for the nuclides and reactions under consideration in the same multi-group energy structure. The Sandwich formula [7] was used to propagate the covariance matrix from the nuclear data to the k_{eff} variance. It is given by

$$\Sigma_k = S_{k,\sigma}^T \cdot \Sigma_\sigma \cdot S_{k,\sigma}, \quad (9)$$

in which Σ_k is the covariance matrix on k_{eff} for the nuclear systems under consideration. The nuclear data which is not being adjusted is not included in the covariance matrix or sensitivity profiles and therefore, only the remaining nuclear data uncertainties are propagated. The remaining variance is then added to the experimental variance. This ensures the nuclear data adjustment is not correcting for bias in other nuclear data. However, it also makes the integral experiments less informative since they are heavily subjected to nuclear data coming from fuel materials.

3 Description of cases

3.1 Chromium-53

Chromium is an isotope that is used frequently in nuclear reactors, more specifically in stainless steel in order to increase its corrosion resistance (11-26%). This, together with the scattering and capture cross sections being significant, makes it an element important for criticality safety in some nuclear systems [8]. A major nuclide of chromium with a relatively poor estimation of the cross section is ^{53}Cr in the 1-10 keV range. Several microscopic measurements exist which measure the capture yield, most notably Guber (2011) and Stieglitz (19xx). However, these experiments are not very consistent with the data available in evaluated nuclear data libraries. In a recent study by Perez-Maroto et al. (2025), new capture yield measurements were performed with a thin sample. It is seen as a possibility to observe whether integral experiments sensitive to Cr-53 in the 1-10 keV range can be used in a Bayesian framework to increase the confidence in the nuclear data of ^{53}Cr .

Several integral experiments were previously identified as candidates, see [9], however, in this paper the criticality experiments PMI-002 and HMI-001 were selected due to their significant sensitivity in the 1-10 keV range, as can be seen in Figure 1 in which the calculated sensitivity to Cr-53 capture is shown for PMI-002 and HMI-001.

In this paper, only the Γ_γ at 4 keV was inferred due to this being the most sensitive Γ_γ -width affecting criticality. The E_r and Γ_n were not perturbed as they are more easily derived from transmission measurements. In this sense, this inference problem is quite trivial since we are only inferring a single parameter and the criticality experiments behave linearly with respect to

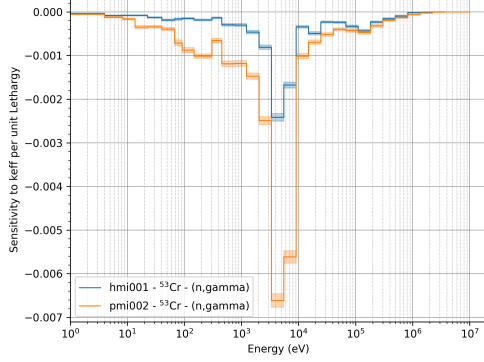


Figure 1: Sensitivity profiles for two criticality experiments sensitive to Cr-53 (n,γ)

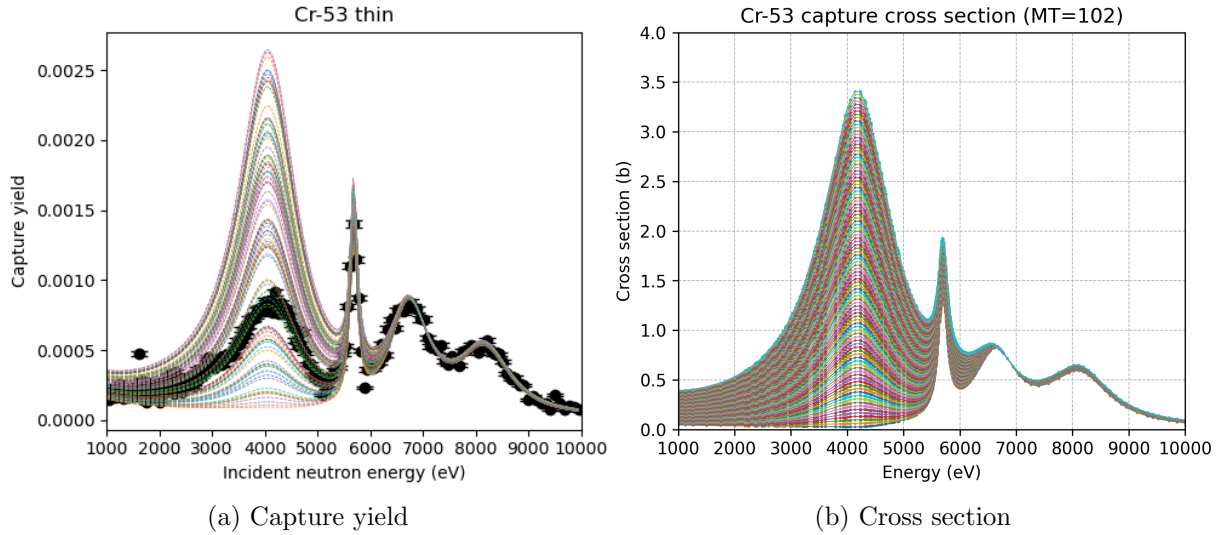


Figure 2: Random samples for capture yield (A) and cross section (B).

changes in Γ_γ , however this is taken as a case study. The perturbation of first Γ_γ -width can be seen in Figure 2 for (a) the capture yield and (b) the cross section.

4 Results and discussions

4.1 Chromium-53

In Figure 3, the validation of the Gaussian Process is shown for (a) the microscopic experiment and (b) an integral experiment.

Several possibilities are now identified, being the case in which only the integral experiments are included, then only microscopic experiment, then both microscopic and integral in which the microscopic experiment is included as in Eq. 7 and as in Eq. 8. The results are shown in Table 1.

In Figure x, the prior and posterior distribution can be found for case 4 in which the Figure 4. It is important to note that in these.

In contrast, when the datapoints are considered independent from each other, the weight of the microscopic datapoints increases heavily. This can be seen in Fig. 4.

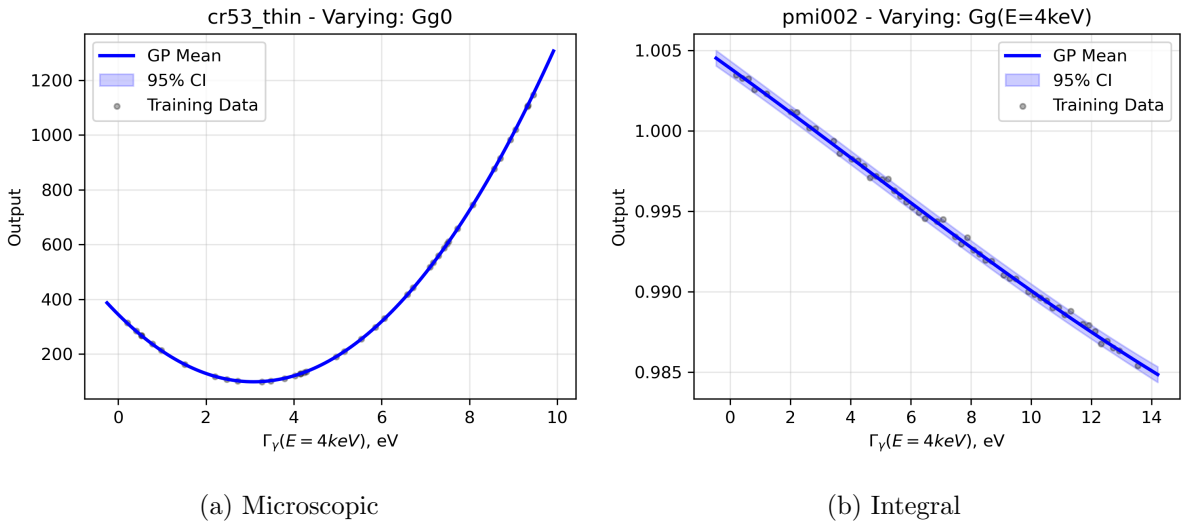


Figure 3: GPs for microscopic (A) and integral (B) experiment.

Table 1: Overview of posterior mean and uncertainty for different combinations of experiments included.

Case	PMI002	HMI001	ntof (ind.)	mean	r. unc. (%)
1				4.14	5.0
2	✓	✓		4.16	4.9
3			✓	3.59	4.1
4	✓	✓	✓	3.60	4.0
5(ind.)	✓	✓	✓	3.09	2.3

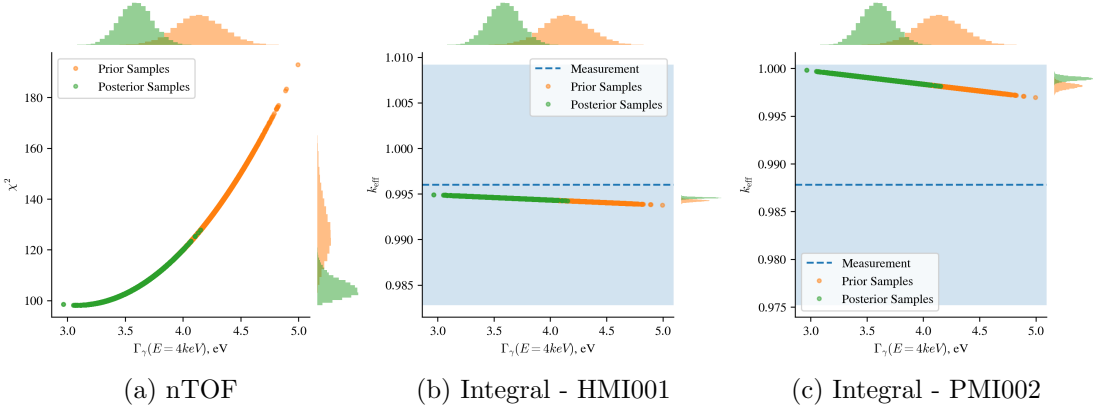


Figure 4: GPs for microscopic (A) and integral (B) and (C) experiments.

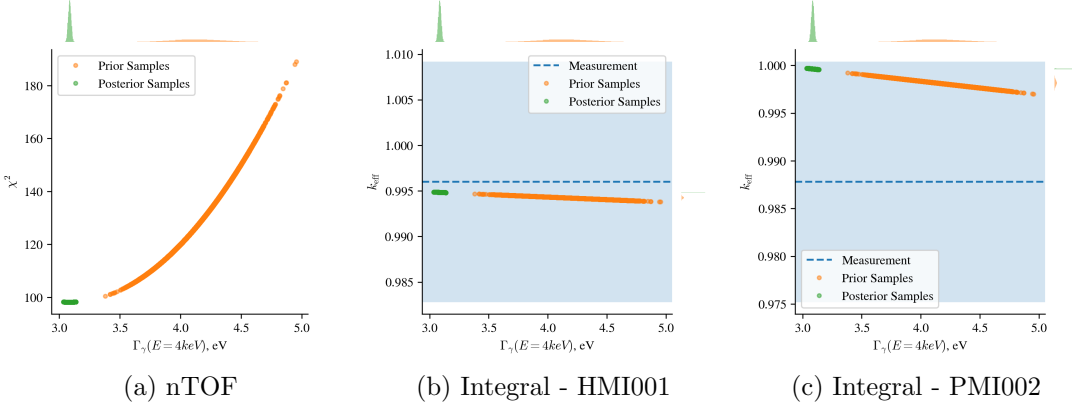


Figure 5: GPs for microscopic (A) and integral (B) and (C) experiments.

5 Conclusions and future work

6 Acknowledgments

References

- [1] N. M. Larson, “Updated User’s Guide for Sammy: Multilevel R-Matrix Fits to Neutron Data Using Bayes’ Equations.”
- [2] J. Leppänen, M. Pusa, T. Viitanen, V. Valtavirta, and T. Kaltiaisenaho, “The Serpent Monte Carlo code: Status, development and applications in 2013,” *Annals of Nuclear Energy*, vol. 82, pp. 142–150, Aug. 2015.
- [3] D. Foreman-Mackey, D. W. Hogg, D. Lang, and J. Goodman, “emcee: The mcmc hammer,” *Publications of the Astronomical Society of the Pacific*, vol. 125, p. 306–312, Mar. 2013.
- [4] M. Aufiero, A. Bidaud, M. Hursin, J. Leppänen, G. Palmiotti, S. Pelloni, and P. Rubiolo, “A collision history-based approach to sensitivity/perturbation calculations in the continuous energy Monte Carlo code SERPENT,” *Annals of Nuclear Energy*, vol. 85, pp. 245–258, Nov. 2015.
- [5] L. Fiorito, J. Dyrda, and M. Fleming, “JEFF-3.3 covariance application to ICSBEP using SANDY and NDAST,” *EPJ Web of Conferences*, vol. 211, p. 07003, 2019.
- [6] D. W. Muir, R. M. Boicourt, A. C. Kahler, J. L. Conlin, and W. Haeck, “The NJOY Nuclear Data Processing System, Version 2016,”
- [7] B. L. Broadhead, B. T. Rearden, C. M. Hopper, J. J. Wagschal, and C. V. Parks, “Sensitivity- and Uncertainty-Based Criticality Safety Validation Techniques,” *Nuclear Science and Engineering*, vol. 146, pp. 340–366, Mar. 2004.
- [8] A. Trkov, O. Cabellos, and R. Capote, “Sensitivity of selected benchmarks to Cr-53 and Cr-50 capture,”
- [9] G. Nobre, M. Pigni, D. Brown, R. Capote, A. Trkov, K. Guber, R. Arcilla, J. Gutierrez, A. Cuadra, G. Arbanas, B. Kos, D. Bernard, and P. Leconte, “Newly Evaluated Neutron Reaction Data on Chromium Isotopes,” *Nuclear Data Sheets*, vol. 173, pp. 1–41, Mar. 2021.